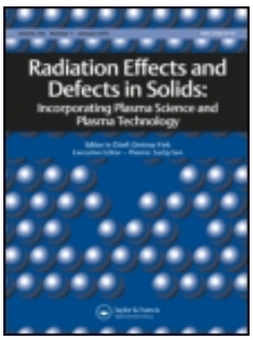

Radiation Effects & Defects in Solids: Incorporating Plasma Science & Plasma Technology

ISSN: 1042-0150 (Print) 1029-4953 (Online) Journal homepage: http://www.tandfonline.com/loi/grad20

On the interface states and series resistance profiles of (Ni/Au)–$Al_{0.22}Ga_{0.78}N$/AlN/GaN heterostructures before and after ^{60}Co (γ-ray) irradiation

S. Demirezen , Ş. Altındal , S. Özçelik & E. Özbay

To cite this article: S. Demirezen , Ş. Altındal , S. Özçelik & E. Özbay (2010) On the interface states and series resistance profiles of (Ni/Au)–$Al_{0.22}Ga_{0.78}N$/AlN/GaN heterostructures before and after ^{60}Co (γ-ray) irradiation, Radiation Effects & Defects in Solids: Incorporating Plasma Science & Plasma Technology, 165:12, 920-929, DOI: 10.1080/10420150.2010.487905

To link to this article: https://doi.org/10.1080/10420150.2010.487905

Published online: 09 Jun 2010.

Radiation Effects & Defects in Solids: Incorporating Plasma Science & Plasma Technology
Vol. 165, No. 12, December 2010, 920–929

Taylor & Francis
Taylor & Francis Group

On the interface states and series resistance profiles of (Ni/Au)–$Al_{0.22}Ga_{0.78}N$/AlN/GaN heterostructures before and after ^{60}Co (γ-ray) irradiation

S. Demirezen[a]*, Ş. Altındal[a], S. Özçelik[a] and E. Özbay[b,c]

[a]*Department of Physics, Faculty of Science and Arts, University of Gazi, Teknikokullar, 06500 Ankara, Turkey;* [b]*Nanotechnology Research Center, Bilkent University, Bilkent, 06800 Ankara, Turkey;* [c]*Department of Physics and Department of Electrical and Electronics Engineering, Bilkent University, Bilkent, 06800 Ankara, Turkey*

(*Received 30 January 2010; final version received 5 April 2010*)

The values of interface states (N_{SS}) and series resistance (R_S) of (Ni/Au)–$Al_{0.22}Ga_{0.78}N$/AlN/GaN heterostructures were obtained from admittance and current–voltage measurements before and after 250 kGy ^{60}Co irradiation. The analyses of these data indicate that the values of capacitance and conductance decrease, as the R_S increases with increasing dose rate due to the generation of N_{SS}. The increase in R_S with increasing dose rate was attributed to two main models. According to the first model, it has been attributed to a direct decrease in the donor concentration in semiconductor material as a result of the elimination of shallow donor states. According to the second model, it is a result of irradiation because of the formation of deep acceptor centers in the semiconductor bulk, and electrons from the shallow donor centers are captured by these acceptors.

Keywords: radiation effect; interface states; series resistance; admittance technique; I–V measurements

1. Introduction

In real metal semiconductor (MS), metal insulator semiconductor (MIS) and high electron mobility transistors (HEMTs), localized interface states exist at the metal/semiconductor (M/S) interface. Therefore, the behavior of these devices is different from the ideal case due to interface states. The reason for their existence is the interruption of the periodic lattice structure at the surface (*1–5*). Due to a number of unique properties, AlGaN/GaN structures are very promising for high-power and radiation-resistant microwave devices, particularly for HEMTs. Also, gallium nitride (GaN) and related wide band gap semiconductor alloys are important for the fabrication of microelectronic devices and are capable of reliable operation at high-power/bias voltage levels, and in high-energy radiation environments (*6–11*). These devices find their main applications in significant radiation exposure involving fields such as aerospace, military and nuclear applications. Studying the effect

*Corresponding author. Email: s.demirezen@gazi.edu.tr

ISSN 1042-0150 print/ISSN 1029-4953 online

DOI: 10.1080/10420150.2010.487905
http://www.informaworld.com

of radiation has been of interest to us, especially the electrical properties of semiconductor devices. In satellite communication, these semiconductor devices have been exposed to rays. Since GaN-based semiconductors are exposed to high-energy particles such as ^{60}Co (γ-ray), high electrons, neutrons or ions, lattice defects arising under these radiations could give new information about the carrier conduction and polarization effect in such devices. These defects act as recombination centers in trapping the generated carriers. A survey of the literature reveals that a large number of studies have been reported on the effect of radiation on MS, MIS and HEMT structures (*12–22*). The origins of these radiation-induced defects are not clearly understood, and thus further studies are necessary to clarify the atomic structure of the defects. Therefore, it is interesting to investigate the radiation damage defect centers introduced by irradiation and to study their effects on the performance of these types of structures. Further, improvements in radiation resistance of these structures are necessary for their widespread application.

The radiation response of the MS, MIS and HEMTs involves several different processes, each with its own dependence on relaxation time, frequency, applied bias voltage, temperature, and so on. Therefore, the overall radiation response of an MIS device is extremely complex. The ionizing radiation interacts with the semiconductor to produce electron–hole pairs. Depending on the kind of radiation incident and on the applied bias voltage/electric field, some fraction of these electron–hole pairs will undergo an initial recombination process (*12, 14*). It is well known that the electrons are much more mobile than the holes at the M/S interface. Thus, electrons are either recombined with the holes or swept out of the insulator by the applied electric field in a time on the order of 1 ps (*12, 14, 19, 23*), but the holes remain near their point of origin. Since high-frequency ($f \geq 500$ kHz) C–V and G/w–V measurements are relatively easily and rapidly carried out, they could yield interesting and meaningful results.

In this study, we focus on the radiation-induced interface states and series resistance effect on admittance (C–V and G/w–V) and I–V characteristics of the (Ni/Au)–$Al_{0.22}Ga_{0.78}N$/AlN/GaN heterostructures at room temperature before and after irradiation. The analysis of these data prove that there is a reaction for extra recombination centers in the case of devices exposed to ^{60}Co (γ-ray) radiation under zero bias. The density of interface states profile was obtained from the high–low-frequency capacitance method after irradiation. The main effect of the gamma radiation is the generation of interface states with the energy level being within the forbidden band gap and at the M/S interface. In addition, the measurement capacitance (C) and conductance (G/ω) are corrected for the series resistance (R_S) effect.

2. Experimental

The samples investigated in the present study were grown on C-face (0001) sapphire (Al_2O_3) substrate by a low-pressure MOCVD reactor. Hydrogen was used as the carrier gas and trimethylgallium (TMGa), trimethylaluminum (TMAl) and ammonia (NH_3) were used as Ga, Al and N precursors, respectively. Prior to the epitaxial growth, the substrate was cleaned in H_2 ambient at 1100 °C. As shown in Figure 1, a 15 nm low-temperature (LT) AlN nucleation layer was grown at 840 °C with a 50 mbar reactor pressure. After the deposition of the LT-AlN nucleation layer, the wafers were heated to a high temperature (HT) for annealing. For the samples, an approximately 0.60 μm HT-AlN buffer layer was deposited on the annealed nucleation layers at 1127 °C with a 400 nm/h growth rate. After the deposition of buffer layers, an approximately 1.9 μm HT-GaN layer was grown at 1040 °C. Finally, a 1.5 nm thick AlN interlayer, a 27 nm thick $Al_{0.22}Ga_{0.78}N$ barrier layer and a 3 nm GaN cap layer were grown at 1080 °C. All layers were nominally undoped.

For the contacts, since the sapphire substrate is insulating, the ohmic and Schottky contacts were made on the top surface. The ohmic contacts were prepared by the evaporation deposition of

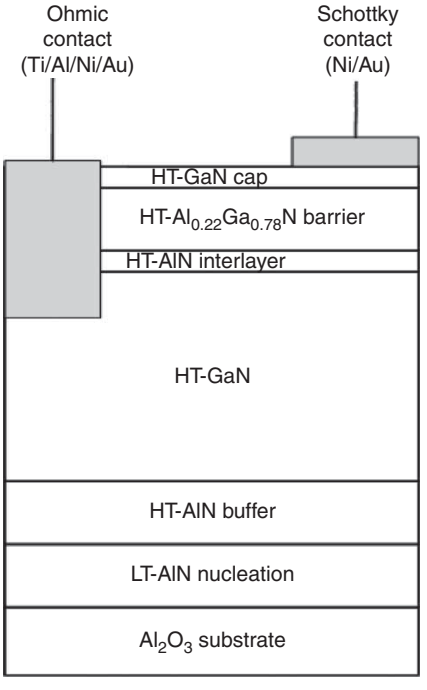

Figure 1. Schematic diagram of the (Ni/Au)/$Al_{0.22}Ga_{0.78}N$/AlN/GaN heterostructure and a view of ohmic and Schottky contacts on the structures.

Ti/Al/Ni/Au (200 Å/2000 Å/300 Å/700 Å). After the metallization step, the contacts were annealed at 850 °C for 30 s in N_2 ambient in order to form the ohmic contact. The Schottky contacts were prepared by the evaporation deposition of Ni/Au (300 Å/500 Å). Both the ohmic and Schottky contacts were made on the top surface as 1.5 mm diameter circular dots. The forward and reverse bias I–V measurements were performed by the use of a Keithley 2400 source meter. The C–V and G–V measurements were carried out using an HP 4192A LF impedance analyzer at 500 kHz. All measurements were performed in the dark before and after ^{60}Co γ-ray source irradiation, and the total dose range was 0–250 kGy at room temperature.

3. Results and discussion

3.1. *Radiation-dependent C–V and G/w–V characteristics*

The C–V and G/w–V characteristics of the (Ni/Au)–$Al_{0.22}Ga_{0.78}N$/AlN/GaN heterostructures, before and after γ-ray irradiation, in the dose range of 0–250 kGy at 500 kHz are shown in Figure 2(a) and (b), respectively. The three distinct regimes of inversion–depletion–accumulation before and after γ-ray irradiation are shown in Figure 2(a). Both the C and G/ω values decrease with increasing dose rate. As shown in Figure 2(a), the C–V curve shifts towards the negative bias voltage with increasing irradiation dose and gives two peaks at depletion and accumulation regions, respectively. The magnitude of these peaks decreases with increasing dose rate. The irradiation dispersion in C decreases with increasing bias voltage. Contrary to the C value, the G/ω value increases with increasing bias voltage. The admittance method (C–V and G/ω–V) is based on conductance losses resulting from the exchange of the majority carriers between the interface states and the majority carrier band of the semiconductor when a small AC signal is

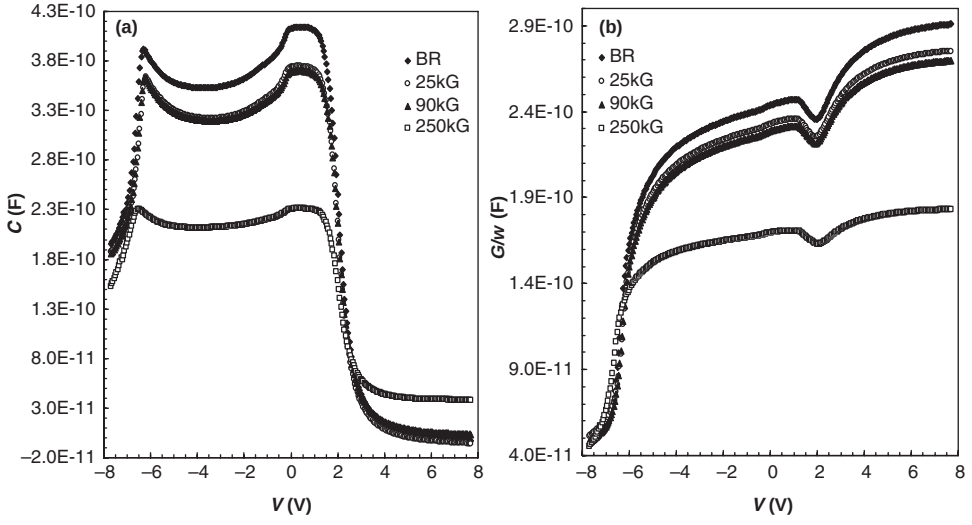

Figure 2. C–V and G/w–V characteristics of (Ni/Au)/$Al_{0.22}Ga_{0.78}N$/AlN/GaN heterostructures under different doses measured at 500 kHz.

applied to the MIS-type devices (*1*, *4*). These applied AC signals cause the Fermi level to oscillate about the mean positions governed by the DC bias voltage, when the device is in the depletion mode.

The magnitude of the series resistance (R_S), which is the most important parameter, causes the main electrical parameters. In order to extract the real R_S of MIS-type structures, several methods have been suggested in the literature (*4*, *24–26*). In our calculations, we have applied the method by Nicollian and Goetzberger (*4*). At sufficiently high frequencies ($f \geq 500$ kHz), the interface states cannot follow the AC signal because at high frequencies the carrier lifetime (τ) is larger than the measured period. Then, the admittance using the parallel RC circuit (*4*, *27*) is equivalent to the total circuit admittance Y_m in the accumulation, as:

$$Y_m = \frac{1}{Z_m} = G_m + jwC_m, \tag{1}$$

where C_m and G_m represent the measured capacitance and conductance in the strong accumulation region. Comparing the real and imaginary parts, R_S can be obtained:

$$R_s = \frac{G_m}{G_m^2 + (\omega C_m)^2}. \tag{2}$$

In addition, the bias voltage dependence of the R_S can be obtained from the measurements of radiation-dependent C–V and G/ω–V data. The R_S values of the (Ni/Au)/$Al_{0.22}Ga_{0.78}N$/AlN/GaN heterostructures were calculated from Equation (2) as a function of gate voltage before and after 250 kGy ^{60}Co (γ-ray) irradiation for 500 kHz (Figure 3). As seen in Figure 3, in depletion and inversion regions, the value of the R_S generally increases with increasing radiation dose and gives a peak at about 3 V, depending on the radiation dose, and disappears at a high dose. It is clearly seen that the value of R_S is dependent on both the applied bias voltage and radiation dose and changes from region to region. Such a behavior of R_S may be attributed to trap charges having enough energy to escape from the traps located at the M/S interface in the semiconductor band gap. Similar results have been reported in the literature (*17*, *28–31*). Titov et al. (*28*) showed that ion irradiation changes not only the concentration of free carriers but also the value of mobility of carriers in GaN semiconductors. They also showed that both the carrier concentration and series

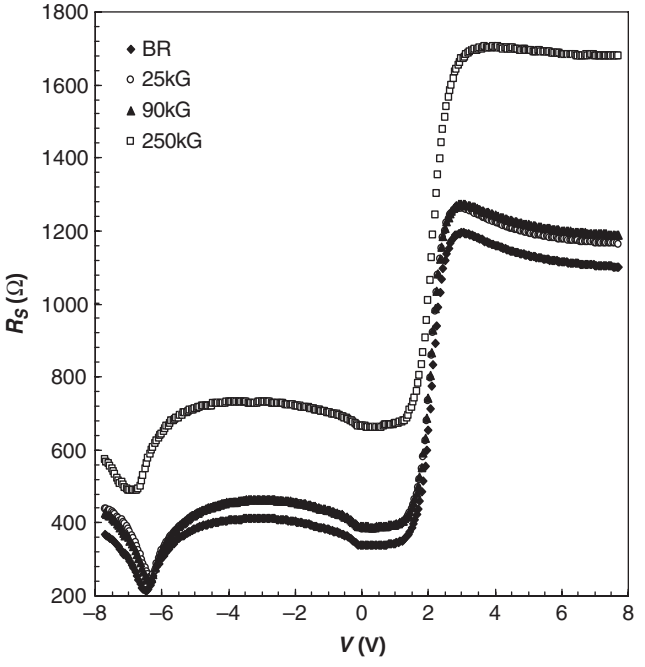

Figure 3. The voltage dependence of the R_S obtained from C–V and G/w–V data under different doses for 500 kHz at room temperature.

resistance of the device increase with increasing doses. In addition, Feteha et al. (*31*) showed that the value of ideality factor (n) and series resistance (R_s) values of a metal insulator semiconductor solar cell increase with increasing dose rate due to an increase in radiation-induced defects. This degradation could be due to the creation of a radiation defect which compensates for the positive charges at the oxide/semiconductor interface and consequently leads to a reduction in the cell efficiency through a reduction in the barrier height at the M/S interface. In light of the above discussions, the increase in R_S with increasing dose rate was attributed to two main models. According to the first model, it has been attributed to a direct decrease in the donor concentration in a semiconductor material as a result of the elimination of shallow donor states. According to the second model, it is a result of irradiation because of the formation of deep acceptor centers in the semiconductor bulk, and electrons from the shallow donor centers are captured by these acceptors.

In order to obtain the real diode capacitance and conductance, the high frequency (500 kHz) measured under forward and reverse biases at room temperature was corrected for the effects of R_S by using Equations (3) and (4), respectively, and is given in Figures 4(a) and (b), respectively:

$$C_c = \frac{[G_m^2 + (\omega C_m)^2]C_m}{a^2 + (\omega C_m)^2} \tag{3}$$

and

$$G_c = \frac{[G_m^2 + (\omega C_m)^2]a}{a^2 + (\omega C_m)^2}, \tag{4}$$

where $a = G_m - [G_m^2 + (\omega C_m)^2]R_s$; C_m and G_m are the measured capacitance and conductance, respectively. When the correction was made on the C–V and G/ω–V plots for the effect of R_S, the values of corrected capacitance (C_c) increased with increasing bias voltage between −6 and −2 V. On the other hand, the value of C in the strong accumulation and inversion regions is

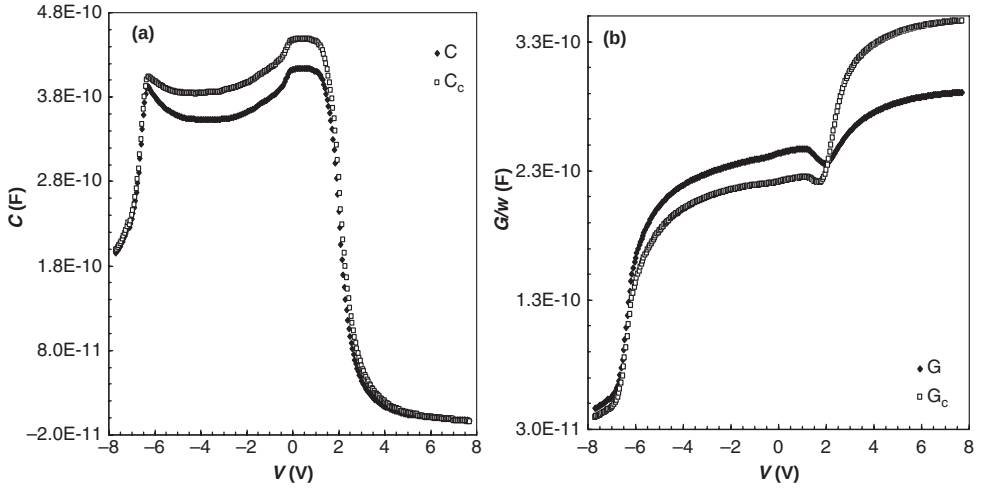

Figure 4. The voltage-dependent plot of (a) the corrected capacitance curves for 500 kHz at room temperature and (b) the corrected conductance curves for 500 kHz at room temperature.

independent of radiation. Conversely, the G_m/w–V and G_c/w–V plots exhibit an intersection behavior at about 2 V.

Figure 5 shows the density distribution profile of interface states (N_{SS}) obtained from before and after irradiation measurement capacitance at 500 kHz using the following formula:

$$D_{it} = \frac{1}{qA}\left[\left(\frac{1}{C_{BR}} - \frac{1}{C_{ox}}\right)^{-1} - \left(\frac{1}{C_{AR}} - \frac{1}{C_{ox}}\right)^{-1}\right], \tag{5}$$

where A is the area of the Schottky contact, q is the elementary electrical charge, C_{ox} is the capacitance of oxide, C_{BR} is measured capacitance before radiation and C_{AR} is measured capacitance after radiation. The advantage of this method comes from the fact that it permits determination of many properties of the insulating interface layer, the semiconductor substrate and interface easily. In this method (*32*), the interface state density is extracted from its capacitance contribution to the measured experimental C–V curve. Before radiation, there is no contribution to the total capacitance due to radiation-induced interface states. As seen in Figure 5, the N_{SS}–V plot gives two peaks at about -6 and $+1$ V values, respectively. Such behaviors of N_{SS} have been attributed to the particular distribution of the interface states at the M/S interface and in the semiconductor band gap and their reordering and restructuring after irradiation. The N_{SS} distributions with peaked structure have also been observed previously (*33–36*).

3.2. *Radiation-dependent I–V characteristics*

The forward and reverse bias I–V characteristics of the (Ni/Au)/$Al_{0.22}Ga_{0.78}N$/AlN/GaN heterostructures before and after irradiation are shown in Figure 6. As shown in Figure 6, the effect of irradiation is clear, especially at the reverse bias region. On the other hand, both I–V characteristics show that they are dominated by the series resistance at higher voltage values. It is seen that after γ-irradiation in the structure, the leakage current has been decreased. The forward bias I–V characteristics before and after irradiation is linear at a value between 0.1 and 0.8 V. In contrast to the low bias region, the I–V curves deviate considerably from linearity due to the effect of R_S when the applied bias voltage is sufficiently large ($V \geq 1$ V). Also, there is an interesting feature

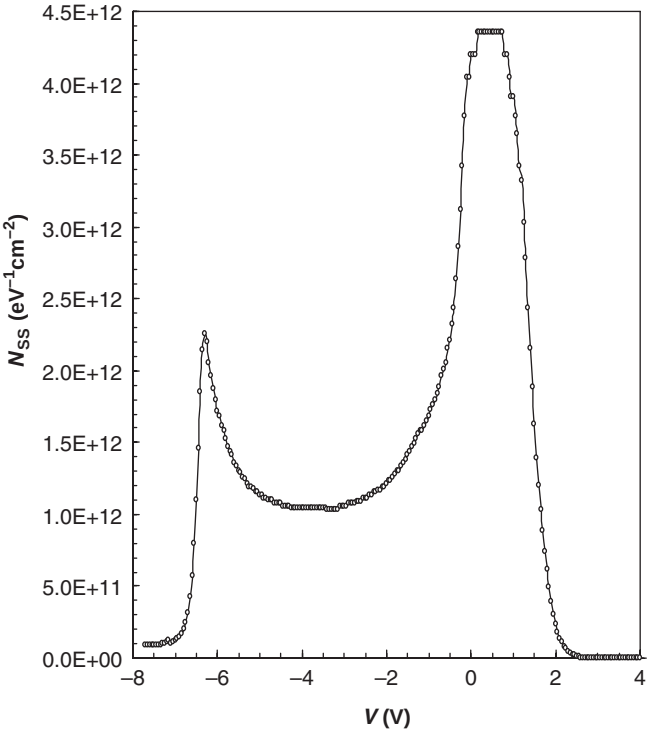

Figure 5. The density distribution profile of N_{SS} obtained from before and after irradiation C–V measurements.

of the forward bias I–V plots: the intersection point at about 1.34 V. It was found that the presence of R_S in the diode causes bending due to current saturation. Chand (*37*) reported that this crossing of forward bias ln I–V plots for a homogeneous Schottky diode can only be realized in plots with zero R_S. Also, Osvald (*38*) showed theoretically that the existence of the R_S is a necessary condition of intersection ln I–V curves. For our sample, the value of R_S is shown to play a crucial role in effecting forward bias I–V plots of the (Ni/Au)/$Al_{0.22}Ga_{0.78}N$/AlN/GaN heterostructures and shows the intersection behavior of the forward bias ln I–V plots. This behavior of the crossing of ln I–V plots appears as an abnormality when seen with respect to the conventional behavior of Schottky barrier diodes.

The measured forward bias I–V characteristics before and after irradiation were analyzed according to the Schottky barrier thermionic emission theory ($V > 3kT/q$), as (*3*, *5*):

$$I = AA^*T^2 \exp\left(-\frac{q\Phi_{bo}}{kT}\right)\left[\exp\left(\frac{q(V - IR_S)}{nkT}\right) - 1\right], \tag{6}$$

where A is the diode area, A^* is the Richardson constant and equals 31.45 A/cm^2 K^2 for (Ni/Au)/$Al_{0.22}Ga_{0.78}N$/AlN/GaN, q is the electron charge, V is the applied bias voltage, the IR_S term is the voltage drop across R_S of the structure, k is the Boltzmann constant, T is the temperature in Kelvin, n is the ideality factor, which is determined from the slope of the linear region of the forward bias ln I–V characteristic through the relation:

$$n = \frac{q}{kT}\frac{dV}{d(\ln I)}. \tag{7}$$

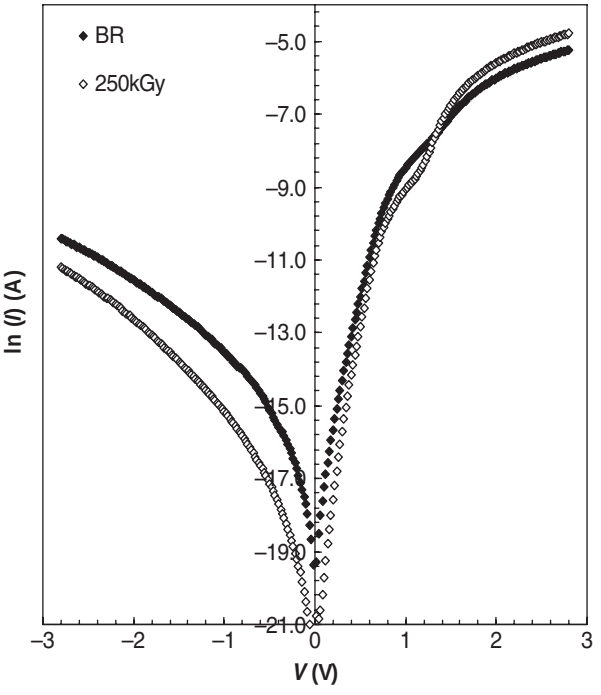

Figure 6. The forward and reverse bias I–V characteristics of (Ni/Au)/$Al_{0.22}Ga_{0.78}N$/AlN/GaN heterostructure before and after irradiation.

The ideality factor refers to the linear part of characteristics where R_S can be assumed to be equal to zero. Also, the value of n is equal to unity for an ideal diode. However, the values of n are greater than unity, and these high values of n can be attributed to the presence of the interfacial thin native insulator layer, to a wide distribution of low Schottky barrier height (SBH) patches, interface states and bias voltage dependence of the SBH (*2*, *3*, *5*, *22*, *39*). The value of reverse bias saturation current (I_0) is determined from the straight line intercept of $\ln(I)$ at zero bias and is given by:

$$I_0 = AA^*T^2 \exp\left(\frac{-q\Phi_{bo}}{kT}\right). \tag{8}$$

The value of zero-bias barrier height (Φ_{bo}) was calculated from Equation (8) as:

$$\Phi_{bo} = \frac{kT}{q} \ln\left(\frac{AA^*T^2}{I_0}\right). \tag{9}$$

The change in I_0, n and Φ_{bo} before and after irradiation was found to be 7.6×10^{-9} A, 2.60 and 0.74 eV and 0.39×10^{-9} A, 1.93 and 0.82 eV, respectively. These results show that the values of I_0 and n decrease with increasing dose rate, but the values of Φ_{bo} increase with increasing dose rate. It is clear that an apparent increase in the Φ_{bo} agrees with those in the literature (*10*, *17*, *22*). In addition, R_S versus V plots before and after irradiation were calculated by taking the derivate (dV/dI) of the resulting plots, which are shown in Figure 7. As shown in Figure 7, at sufficiently high forward bias, the structure resistance approaches a constant value, and this value is the R_S. On the other hand, structure resistance is also a constant value at sufficiently high reverse bias, and this value is the structure shunt resistance (R_{sh}). The analysis of both the admittance (C–V and G/w–V) and I–V data (except for after the intersection point) indicates that the values of R_S have increased after γ-irradiation. This increase can be attributed to the irradiation-induced

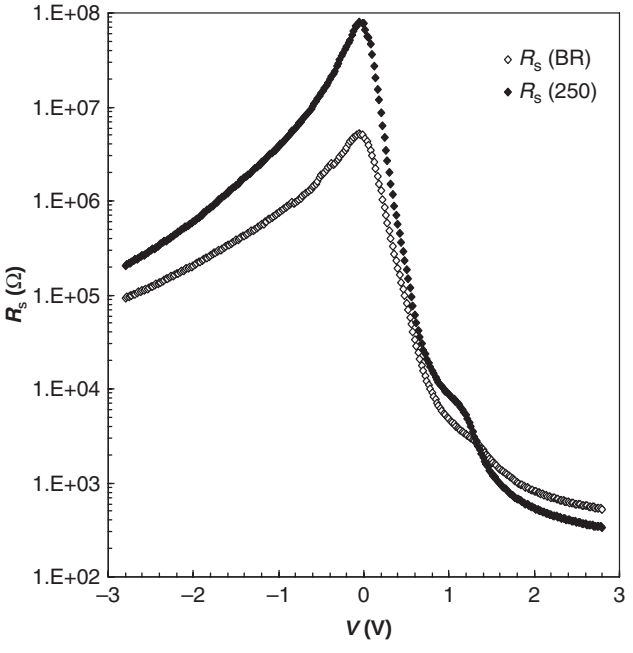

Figure 7. The R_S–V plots of the (Ni/Au)/$Al_{0.22}Ga_{0.78}N$/AlN/GaN heterostructures obtained from I–V data before and after irradiation.

defects because the defects are created in the crystal lattice due to γ-irradiation. Similar results have been obtained recently in the literature for Schottky barrier diodes (*22, 31, 40, 41*).

4. Conclusion

The effect of ^{60}Co (γ-ray) irradiation on the electrical characteristics of (Ni/Au)–$Al_{0.22}Ga_{0.78}N$/AlN/GaN heterostructures has been investigated using admittance (C–V and G/ω–V) and I–V measurements at room temperature. The values of C and G/ω decreased with an increase in dose rate. The measurements of C and G/ω are corrected for the effect of R_S. The bias voltage-dependent density distribution of the N_{SS} profile of the (Ni/Au)–$Al_{0.22}Ga_{0.78}N$/AlN/GaN heterostructures was obtained from before and after C–V measurements. In addition, the bias voltage-dependent R_S profile of the (Ni/Au)–$Al_{0.22}Ga_{0.78}N$/AlN/GaN heterostructures was obtained from both the admittance spectroscopy method (C–V and G/w–V) and I–V measurements in the forward and reverse bias regions before and after irradiation. Experimental results show that the value of the R_S generally increases with increasing radiation, especially at the reverse bias region. On the other hand, the R_S value is dependent on both the applied bias voltage and radiation dose, and changes from region to region. This increase can be attributed to the irradiation-induced interface states in the semiconductor crystal after irradiation. It is clearly shown that we may easily derive the voltage-dependent R_S values from these two methods. In particular, the admittance technique is based on DC bias voltage-dependent complex admittance measurements at a fixed frequency and temperature. The main advantage of these two methods is that they are very easy to use and yield an accurate set of information on variation of N_{SS} and R_S. In conclusion, the main effect of the radiation is the generation of interface states with energy level within the forbidden band gap and at the M/S interface.

References

(1) Nicollian, E.H.; Goetzberger, A. *Appl. Phys. Lett.* **1965,** *7* (8), 216–219.
(2) Card, H.C.; Rhoderick, E.H. *J. Phys. D* **1971**, *4*, 1589–1601.
(3) Sze, S.M. *Physics of Semiconductor Devices*, 2nd ed., Wiley: New York, 1981.
(4) Nicollian, E.H.; Brews, J.R. *MOS (Metal/Oxide/Semiconductor) Physics and Technology*; Wiley: New York, 1982.
(5) Rhoderick, E.H.; Williams, R.H. *Metal Semiconductor Contacts*, 2nd ed.; Clarendon Press: Oxford, 1988.
(6) Lisesivdin, S.B.; Demirezen, S.; Caliskan, M.D.; Yildiz, A.; Kasap, M.; Ozcelik, S.; Ozbay, E. *Semicond. Sci. Technol.* **2008,** *23*, 095008-1–6.
(7) Mishra, U.K.; Wu, Y.F.; Keller, B.P.; Denbaars, S.P. *IEEE Trans. Microw. Theory Tech.* **1998**, *46*, 756–761.
(8) Chow, K.H.; Watkins, G.D.; Usui, A.; Mizuta, M. *Phys. Rev. Lett.* **2000,** *85*, 2761–2764.
(9) Umana-Membreno, G.A.; Dell, J.M.; Parish, G.; Nener, B.D.; Faraone, L.; Mishra, U.K. *IEEE Trans. Electron Devices* **2003,** *50*, 2326–2334.
(10) Umana-Membreno, G.A.; Dell, J.M.; Parish, G.; Nener, B.D.; Faraone, L.; Keller, S.; Mishra, U.K. *J. Appl. Phys.* **2007,** *101*, 054511-1–8.
(11) Vitusevich, S.A.; Klein, N.; Belyaev, A.E.; Danylyuk, S.V.; Petrychuk, M.V.; Konakova, R.V.; Kurakin, A.M.; Rengevich, A.E.; Avksentyev, A.Yu.; Danilchenko, B.A.; Tilak, V.; Smart, J.; Vertiatchikh, A.; Eastman, L.F. *Phys. Stat. Sol.* **2003,** *195*, 101–105.
(12) Zaininger, K.H.; Holmes-Seidle, A.G. *RCA Rev.* **1967,** *28*, 208–240.
(13) Gildenblat, G.; Pimbley, J.M.; Cote, M.F. *Appl. Phys. Lett.* **1984,** *45* (5), 558–559.
(14) Oldham, T.R.; McLean, F.B.; Boesch Jr, H.E.; McGarrity, J.M. *Semicond. Sci. Technol.* **1989,** *4*, 986–999.
(15) Jayavel, P.; Kumar, J.; Santhakumar, K.; Magudapathy, P.; Nair, K.G.M. *Vacuum* **2000,** *57*, 51–59.
(16) Chauhan, R.K.; Chakrabarti, P. *Microelectron. J.* **2002,** *33*, 197–203.
(17) Karataş, Ş.; Türüt, A.; Altındal, Ş. *Nucl. Instrum. Methods A* **2005,** *555*, 260–265.
(18) Tataroglu, A.; Altındal, Ş.; Bülbül, M.M. *Nucl. Instrum. Methods A* **2006,** *568*, 863–868.
(19) Winokur, P.S.; Schwank, J.R.; Mcwhorter, P.J.; Dressendorfer, P.V.; Turpin, D.C. *IEEE Trans. Nucl. Sci.* **1984,** *31*, 1453–1460.
(20) Tataroglu, A.; Altındal, Ş. *Nucl. Instrum. Methods A* **2007,** *580*, 1588–1593.
(21) Gullu, O.; Demir, F.; Cimilli, F.E.; Biber, M. *Vacuum* **2008,** *82*, 789–793.
(22) Uğurel, E.; Aydoğan, Ş.; Şerifoğlu, K.; Türüt, A. *Microelectron. Eng.* **2008,** *85*, 2299–2303.
(23) Ma, T.P. *Appl. Phys. Lett.* **1975,** *27*, 615–617.
(24) Norde, H. *J. Appl. Phys.* **1979,** *50*, 5052–5053.
(25) Sato, K.; Yasamura, Y. *J. Appl. Phys.* **1985,** *58*, 3655–3657.
(26) Cheung, S.K.; Cheung, N.W. *Appl. Phys. Lett.* **1986,** *49*, 85–87.
(27) Kwa, K.S.K.; Chattopadhyay, S.; Jankovic, N.D.; Olsen, S.H.; Driscoll, L.S.; O'Niell, A.G. *Semicond. Sci. Technol.* **2003,** *18*, 82–87.
(28) Titov, A.I.; Kucheyev, S.O. *J. Appl. Phys*. **2002,** *92*, 5740–5744.
(29) Götz, W.; Johnson, N.M.; Bremser, M.D.; Davis, R.F. *Appl. Phys. Lett.* **1996,** *69*, 2379–2381.
(30) Legodi, M.J.; Hullavarad, S.S.; Goodman, S.A.; Hayes, M.; Auret, F.D. *Phys. B* **2001**, *308–310*, 1189–1192.
(31) Feteha, M.Y.; Soliman, M.; Gomaa, N.G.; Ashry, M. *Renew. Energy* **2002,** *26*, 113–120.
(32) Castagne, R.; Vapaille, A. *Surf. Sci.* **1971,** *28*, 157–193.
(33) Deuling, H.; Klausmann, E.; Goetzberger, A. *Solid-State Electron.* **1972,** *15*, 559–571.
(34) Kar, S.; Varma, S. *J. Appl. Phys.* **1985,** *58* (11), 4256–4266.
(35) Kar, S.; Narasimhan, R.L. *J. Appl. Phys.* **1987,** *61* (12), 5353–5359.
(36) Hung, K.K.; Cheng, Y.C. *J. Appl. Phys.* **1987,** *62*, 4204–4211.
(37) Chand, S. *Semicond. Sci. Technol.* **2004,** *19*, 82–86.
(38) Osvald, J. *Solid State Commun.* **2006,** *138*, 39–42.
(39) Werner, J.H.; Gűttler, H.H. *J. Appl. Phys.* **1991,** *69*, 1522–1533.
(40) Dökme, İ.; Altındal, Ş. *Semicond. Sci. Tech.* **2006,** *21*, 1053–1058.
(41) Karataş, Ş.; Türüt, A.; Altındal, Ş. *Radiat. Phys. Chem.* **2009,** *78*, 130–134.